


# FREQTSF: TIME SERIES FORECASTING VIA CAPTURING INTRA- AND INTER-VARIABLE VARIATIONS IN THE FREQUENCY DOMAIN

A PREPRINT

 **Rujia Shen**

Faculty of Computing  
Harbin Institute of Technology  
Harbin, Heilongjiang, China  
shenrujia@stu.hit.edu.cn

**Yaoxiong Lin**

Faculty of Computing  
Harbin Institute of Technology  
Harbin, Heilongjiang, China  
23S136168@stu.hit.edu.cn

**Liangliang Liu**

Faculty of Computing  
Harbin Institute of Technology  
Harbin, Heilongjiang, China  
liull@stu.hit.edu.cn

**Boran Wang**

Faculty of Computing  
Harbin Institute of Technology  
Shenzhen, Guangdong, China  
wangboran@hit.edu.cn

**Yi Guan**

Faculty of Computing  
Harbin Institute of Technology  
Harbin, Heilongjiang, China  
guanyi@hit.edu.cn

**Yang Yang**

School of Artificial Intelligence  
Changchun University of Science and Technology  
Changchun, Jilin, China  
yangyang\_hit\_wi@163.com

 **Jingchi Jiang**

The Artificial Intelligence Institute  
Harbin Institute of Technology  
Harbin, Heilongjiang, China  
jiangjingchi@hit.edu.cn

September 23, 2024

## ABSTRACT

Time series forecasting (TSF) plays a crucial role in various applications, including electricity transformation, medical monitoring, and crop growth. Despite the advancements in deep learning methods for TSF, their capacity to predict long-term series remains constrained. This limitation arises from the failure to account for both intra- and inter-variable variations meanwhile. To mitigate this challenge, we introduce the FreqBlock, which leverages a frequency domain perspective to capture intra- and inter-variable variations. After transforming into the frequency domain via the Frequency Transform Module, the Frequency Cross Attention between the real and imaginary parts is designed to obtain enhanced frequency representations and capture intra-variable variations. Furthermore, Inception blocks are employed to integrate information, thus capturing correlations across different variables. Our backbone network, FreqTSF, employs a residual architecture by concatenating multiple FreqBlocks, thereby preventing degradation issues. Theoretically, we demonstrate that FreqTSF achieves a substantial reduction in both time and memory complexity, decreasing from  $\mathcal{O}(L^2)$  to  $\mathcal{O}(L)$  per FreqBlock computation. Empirical evaluations on three benchmark datasets reveal that FreqTSF delivers an overall relative Mean Squared Error (MSE) reduction of 30% and an overall relative Mean Absolute Error (MAE) reduction of 22% when compared to the latest state-of-the-art methods. The implementation code is accessible at <https://github.com/HITshenrj/FreqTSF>.

**Keywords** Time series forecasting · Frequency Transform Module · Frequency Cross Attention · Residual structure · Frequency domain

# 1 Introduction

Time series forecasting (TSF) aims to forecast the future value of time series using their historical values. With the development of deep learning, numerous models have been proposed and achieved superior performance [Wu et al., 2021, Liu et al., 2022, Zhou et al., 2022, Woo et al., 2022, Nie et al., 2023, Liu et al., 2024, Xu et al., 2024]. The application of these models in the real world spans various sectors, such as energy [Alvarez et al., 2010, Mohammed and Al-Bazi, 2022], medical treatment [Li et al., 2021, Khadem et al., 2023], and agriculture [Saini et al., 2020]. These existing models generally either focus on the intra-variable variations by using channel independence [Nie et al., 2023], or simply apply attention in the time or frequency domain to capture inter-variable variations [Wu et al., 2021, Liu et al., 2022, Zhou et al., 2022, Woo et al., 2022, Liu et al., 2024, Xu et al., 2024].

However, mutual influences between variables are of equal importance to intra-variable variations. As illustrated in Figure 1, intra-variable variations refer to the changes within each variable over time, while inter-variable variations denote the mutual influences between different variables. For instance, when predicting blood glucose levels, not only do historical blood glucose values play a role, but historical records of food intake and insulin injections are also critical for determining future blood glucose changes. Previous research [Zhang and Yan, 2023] has attempted to address this issue by exploring and leveraging both intra- and inter-variable dependencies in the time domain. Nonetheless, a potentially more fundamental approach is to directly and simultaneously capture these variations in the frequency domain, enabling the modeling of the intrinsic properties of the time series. This frequency-domain approach can provide a more robust framework for understanding the underlying dynamics of the data, potentially leading to more accurate forecasting.

To capture intra- and inter-variable variations directly and simultaneously, we propose FreqTSF, which shifts our perspective to the **F**requency domain for **T**ime **S**eries **F**orecasting. First, based on the fact that real-world time series often exhibit multi-periodicity, such as daily and annual variations in electricity transformations, unlike other TSF methods [Zhou et al., 2022, Yi et al., 2023] using the Fast Fourier Transform (FFT), we propose to use the Short-Time Fourier Transform (STFT) with predefined windows of varying sizes in the Frequency Transform Module. This approach aims to decouple overlapping and interacting periodic signals, thereby better addressing both intra- and inter-variable variations. Second, inspired by the inherent Kramer-Kronig relations (KKRs) in the frequency domain, we introduce a novel Frequency Cross Attention. This mechanism operates between the real and imaginary parts of the frequency representation, thereby enhancing the frequency representations and capturing intra-variable variations more effectively. Moreover, we employ Inception blocks to extract changes between variables, which further improve the model’s ability to handle inter-variable dependencies. These above components form FreqBlock, which serves as the fundamental building block of FreqTSF. The overall architecture of FreqTSF adopts a residual structure by stacking multiple FreqBlocks. This design not only enhances the model’s capacity to learn complex patterns but also mitigates degradation problems, ensuring robust performance in long-term forecasting tasks.

Our contributions are four-fold:

- Motivated by the inherent KKR in the frequency domain, we develop a modular framework for modeling both intra- and inter-variable variations. Once transforming into the frequency domain, we can present these variations simultaneously.
- We propose FreqTSF, which is built upon residual FreqBlocks. Each FreqBlock first decouples multiple periodic signals using the Short-Time Fourier Transform (STFT), then captures intra-variable variations through Frequency Cross Attention between the real and imaginary parts. Lastly, the FreqBlock employs inception blocks to mix information, capturing correlations between variables effectively.
- We significantly reduce both the time complexity and memory complexity for each FreqBlock computation from  $\mathcal{O}(L^2)$  to  $\mathcal{O}(L)$ , as verified through theoretical analysis and empirical evaluations.

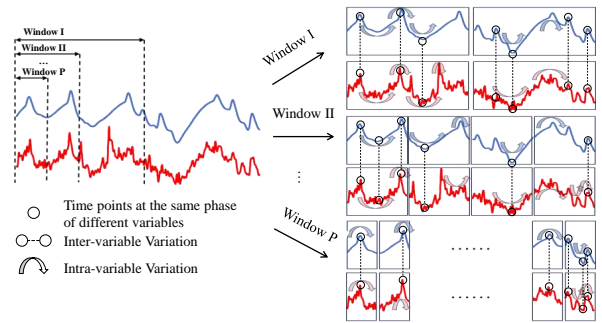


Figure 1: Intra- and inter-variable variations. Intra-variable variations refer to the changes within each variable over time, while inter-variable variations denote the interactions between different variables.

- Experimental results demonstrate that FreqTSF consistently achieves state-of-the-art performance in time series forecasting. The model shows approximately a 30% reduction in Mean Squared Error (MSE) and a 22% reduction in Mean Absolute Error (MAE) compared to existing methods.

## 2 Related Work and Motivation

In this section, we commence by presenting the problem statement, as detailed in Section 2.1. Subsequently, we discuss the cutting-edge TSF methods (Section 2.2), which, despite their remarkable performances, still offer the potential for further refinement. In Section 2.3, we elaborate on the method for converting time-domain information into the frequency domain. Finally, in Section 2.4, we delve into the Kramers-Kronig relations between the real and imaginary components of causal systems in the frequency domain, which serve as both the inspiration and theoretical underpinning of our research.

### 2.1 Problem Statement

The input data points, denoted by  $X = \{x_1^t, \dots, x_D^t\}_{t=1}^L \in \mathbb{R}^{D \times L}$ , are defined as the lookback window of time series, where  $L$  represents the length of the lookback window,  $D \geq 1$  is the number of variables, and  $x_j^t$  is the value of the  $j$ -th variable at the  $t$ -th time step. The task of TSF is to predict the forecasting horizon  $\hat{X} = \{\hat{x}_1^t, \dots, \hat{x}_D^t\}_{t=L+1}^{L+T} \in \mathbb{R}^{D \times T}$  by using the lookback window. In this paper, we specifically focus on multi-step TSF, where  $T > 1$ .

### 2.2 Time Series Forecasting

Many classical methods, such as ARIMA [Box and Jenkins, 1968, Box et al., 2015], followed a Markovian process and constructed autoregressive TSF models based on predefined time patterns. However, this autoregressive process became ineffective in real-world nonlinear and non-stationary conditions.

With the flourishing development of deep neural networks, RNNs, specialized for time series data analysis, have been proposed and achieved remarkable results. The simplest form in the RNN family [Medsker and Jain, 2001] contains a single hidden layer and recurrent connections. However, this form often suffers from the problems of vanishing or exploding gradient, which makes it challenging for long-term series prediction [Bengio et al., 1994]. To address the gradient problems, Long Short-Term Memory (LSTM) [Hochreiter and Schmidhuber, 1997] and Gated Recurrent Unit (GRU) [Chung et al., 2014] employ gated structures to control the flow of information, allowing better handling of dependencies in long sequences. However, due to inherent design flaws, recurrent models still need help adapting to long-term TSF tasks.

With the resounding success of the Transformer architecture in the fields of natural language processing [Vaswani et al., 2017, Kenton and Toutanova, 2019] and computer vision [Dosovitskiy et al., 2020], it has also been refined and adapted for TSF. Autoformer [Wu et al., 2021] introduced an auto-correlation mechanism based on series periodicity, facilitating dependency discovery and representation aggregation at the sub-series level. This innovation enhanced the Transformer’s information utilization and effectively eliminated the information utilization bottleneck. NSformer [Liu et al., 2022] sought to improve the forecasting capability for non-stationary data by introducing series stationarization and de-stationary attention mechanisms, demonstrating its efficacy through theoretical analysis and empirical experiments. To further enhance the accuracy and efficiency of Transformer-based predictions, ETSformer [Woo et al., 2022] leveraged the principle of exponential smoothing. It employed exponential smoothing and frequency attention instead of the self-attention mechanism in traditional Transformers, aiming to improve accuracy and efficiency. PatchTST [Nie et al., 2023] utilized a patching design to preserve local semantic information in the embeddings while concurrently reducing the computation and memory usage of the attention maps quadratically, enabling the model to attend to a longer historical context. To adapt the Transformer for handling longer lookback windows and to eliminate meaningless attention maps, iTransformer [Liu et al., 2024] reconfigured the Transformer architecture by simply applying the attention and feed-forward networks to the inverted dimensions. This modification allowed for more efficient processing of longer sequences and improved attention mechanisms. FEDformer [Zhou et al., 2022] emphasized enhancing the Transformer’s capability to capture the global profile of time series by performing seasonal-trend decomposition in the frequency domain. To improve the Transformer’s ability to model cross-time and cross-dimension dependencies, Crossformer [Zhang and Yan, 2023] initially segmented the time series while preserving both temporal and dimensional information. It then employed a two-stage attention mechanism to capture cross-time and cross-dimension dependencies individually, offering a more nuanced and comprehensive understanding of the time series.

Not only has the Transformer architecture been applied to time series forecasting, but CNN-based methods have also proven highly efficient. TimesNet [Wu et al., 2023] leveraged convolutional neural networks to identify multi-periodicity in time series, effectively extracting complex temporal variations through a parameter-efficient inception block [Szegedy

et al., 2015]. Recently, a series of MLP-based methods have been proposed to reduce model parameters and enhance computational speed while maintaining accuracy. LightTS [Zhang et al., 2022], based on the notion that down-sampling a time series often preserves the majority of its information, used an MLP-based structure to make predictions after down-sampling, significantly reducing computational load without compromising accuracy. DLinear [Zeng et al., 2023] avoided the temporal information loss caused by the permutation-invariant self-attention mechanism by employing a simple one-layer linear model, achieving greater accuracy than Transformer-based models. FreTS [Yi et al., 2023] applied MLPs in the frequency domain, allowing them to have a complete view of signals and more easily learn global dependencies. FITS [Xu et al., 2024] transformed the time series into the complex frequency domain for frequency interpolation and subsequently mapped the interpolation back to the time domain. FITS used a single linear layer to learn the interpolation of complex values.

Although the methods mentioned above effectively predict time series, they overlook intra- and inter-variable variations in the frequency domain, which constrains their capacity to predict long-term time series. Consequently, this paper aims to address this shortcoming by exploring how to simultaneously capture both intra- and inter-variable variations in the frequency domain.

### 2.3 From the Time Domain to the Frequency Domain

A commonly used method for transforming time series data from the time domain to the frequency domain is the Fast Fourier Transform (FFT) [Nussbaumer and Nussbaumer, 1982, Cochran et al., 1967]. The FFT is widely applied because it significantly reduces the computational complexity of the Discrete Fourier Transform [Briggs and Henson, 1995]. In this study, however, we use the Short Time Fourier Transform (STFT) [Cvetkovic, 2000, Durak and Arıkan, 2003] to decouple overlapping and interacting periodic signals, thereby better accounting for intra- and inter-variable variations.

The STFT consists of multiple windows of different sizes, and its fundamental component is the Fourier transform. Therefore, the STFT can be considered a collection of numerous Fourier transforms. The STFT first divides a long time series into shorter segments of equal length and then computes the Fourier transform separately for each segment. As the window slides along the time axis, until it reaches the end, the STFT of the time series is computed, resulting in a two-dimensional representation of the series. Moreover, different window sizes produce multi-scale STFT results.

Mathematically, this process can be expressed as follows:

$$\text{STFT}\{X\}(\omega, \tau) = \sum_{t=1}^L x^t w(t - \tau) e^{-i\omega t}, \quad (1)$$

where  $w(\tau)$  represents the window function, usually a Hann window,  $X$  denotes the time series to transform and  $\omega$  is the angular frequency with  $i^2 = -1$ . The  $\text{STFT}\{X\}$  represents a function that captures the variations of the signal concerning both the time and frequency domain.

### 2.4 The Real and Imaginary Components in the Frequency Domain

In control theory, a causal system is defined as one in which the output depends on past and present inputs but not on future ones [Karimi and Hamilton, 2003]. This relationship aligns with the inherent nature of time series data, where data unfolds sequentially over time, and present data points do not precede future ones. Consequently, in this study, we approximate the inherent mechanism of time series data as a causal system for analysis.

We will subsequently elucidate a theoretical constraint on a causal system in the frequency domain, explicitly concerning the interdependence of the real and imaginary parts as described by the Kramers-Kronig relations [King, 2009]. These relations are pivotal in linking the real and imaginary components of an analytic and causal function. Essentially, they provide integral transforms that describe how the real part of a function can be derived from its imaginary part and vice versa, given the function’s causality and analyticity.

**Theorem 1** *Let  $X(t)$  be a causal time function with respect to time  $t$ , i.e.,  $X(t) = \begin{cases} 0, & t < 0 \\ X(t), & t \geq 0 \end{cases}$ .  $X(t)$  does*

*not contain the continuous-time unit impulse function  $\delta(t) = \begin{cases} 0, & t \neq 0 \\ \infty, & t = 0 \end{cases}$  and derivatives at  $t = 0$ . Suppose the Fourier transform  $\mathcal{F}$  of  $X(t)$  is represented in the form of the real part  $Re$  and the imaginary part  $Im$ , i.e.,  $X(t) \leftrightarrow F(\omega) = Re(\omega) + iIm(\omega)$ . Then, we have:*

$$\begin{aligned}
Re(\omega) &= \frac{1}{\pi} \int_{-\infty}^{\infty} \frac{Im(\sigma)}{\omega - \sigma} d\sigma, \\
Im(\omega) &= -\frac{1}{\pi} \int_{-\infty}^{\infty} \frac{Re(\sigma)}{\omega - \sigma} d\sigma.
\end{aligned} \tag{2}$$

The Equation 2 [Cizek, 1970, Benitez et al., 2001] asserts that for any causal time function, the real and imaginary components of its Fourier transform adhere to the Kramers-Kronig relations (KKRs). These relations establish bidirectional mathematical connections between the real and imaginary parts of complex functions. From Equation 2, it can be observed that the real and imaginary parts exhibit periodic characteristics as a function of  $\omega$ . Moreover, the real and imaginary parts themselves can reflect intra-variable characteristics of time series, thereby making their expression conducive to effective forecasting.

Next, we will demonstrate the Kramers-Kronig relationship within the context of the Short-Time Fourier Transform (STFT) to elucidate the design motivation of our method. Although both frequency and time are localized in STFT, this proof can indirectly validate the rationality and foundation of our model design.

**Lemma 1** *Let  $X(t)$  be a causal time function with respect to time  $t$ , i.e.,  $X(t) = \begin{cases} 0, & t < 0 \\ X(t), & t \geq 0 \end{cases}$ .  $X(t)$  does not contain the continuous-time unit impulse function  $\delta(t) = \begin{cases} 0, & t \neq 0 \\ \infty, & t = 0 \end{cases}$  and derivatives at  $t = 0$ . Suppose the STFT of  $X(t)$  is represented in the form of the real part  $Re$  and the imaginary part  $Im$  with window  $w$ , i.e.,  $X(t) \leftrightarrow STFT(\omega, \tau) = Re(\omega, \tau) + iIm(\omega, \tau)$ . Then, we have:*

$$\begin{aligned}
Re(\omega, \tau) &= \frac{1}{\pi} \int_{-\infty}^{\infty} \frac{Im(\sigma, \tau)}{\omega - \sigma} d\sigma, \\
Im(\omega, \tau) &= -\frac{1}{\pi} \int_{-\infty}^{\infty} \frac{Re(\sigma, \tau)}{\omega - \sigma} d\sigma.
\end{aligned} \tag{3}$$

**Proof 1**  $X(t)$  can be expressed as  $X(t) = X(t)\epsilon(t)$  by introducing the unit step function  $\epsilon(t) = \begin{cases} 1, & t > 0 \\ 0, & t \leq 0 \end{cases}$ . Taking the STFT of both sides of  $X(t) = X(t)\epsilon(t)$ , based on the frequency domain convolution theorem [Weisstein, 2014], we have:

$$\begin{aligned}
STFT\{X(t)\} &= Re(\omega, \tau) + iIm(\omega, \tau), \\
STFT\{X(t)\epsilon(t)\} &= \frac{1}{2\pi} [Re(\omega, \tau) + iIm(\omega, \tau)] \times [\pi\delta(\omega, \tau) + \frac{1}{i\omega}].
\end{aligned} \tag{4}$$

Using  $STFT\{X(t)\} = STFT\{X(t)\epsilon(t)\}$  and then we have:

$$\begin{aligned}
Re(\omega, \tau) + iIm(\omega, \tau) &= \frac{1}{2\pi} [Re(\omega, \tau) + iIm(\omega, \tau)] \times [\pi\delta(\omega, \tau) + \frac{1}{i\omega}] \\
&= [\frac{Re(\omega, \tau)}{2} + \frac{1}{2\pi} Im(\omega, \tau) \times \frac{1}{\omega}] + i[\frac{Im(\omega, \tau)}{2} - \frac{1}{2\pi} Re(\omega, \tau) \times \frac{1}{\omega}].
\end{aligned} \tag{5}$$

Equating the real and imaginary parts on both sides of the equation and rearranging, we get:

$$\begin{aligned}
Re(\omega, \tau) &= \frac{1}{\pi} Im(\omega, \tau) \times \frac{1}{\omega} = \frac{1}{\pi} \int_{-\infty}^{\infty} \frac{Im(\sigma, \tau)}{\omega - \sigma} d\sigma, \\
Im(\omega, \tau) &= -\frac{1}{\pi} Re(\omega, \tau) \times \frac{1}{\omega} = -\frac{1}{\pi} \int_{-\infty}^{\infty} \frac{Re(\sigma, \tau)}{\omega - \sigma} d\sigma.
\end{aligned} \tag{6}$$

So far, the Equation 3 has been proven.

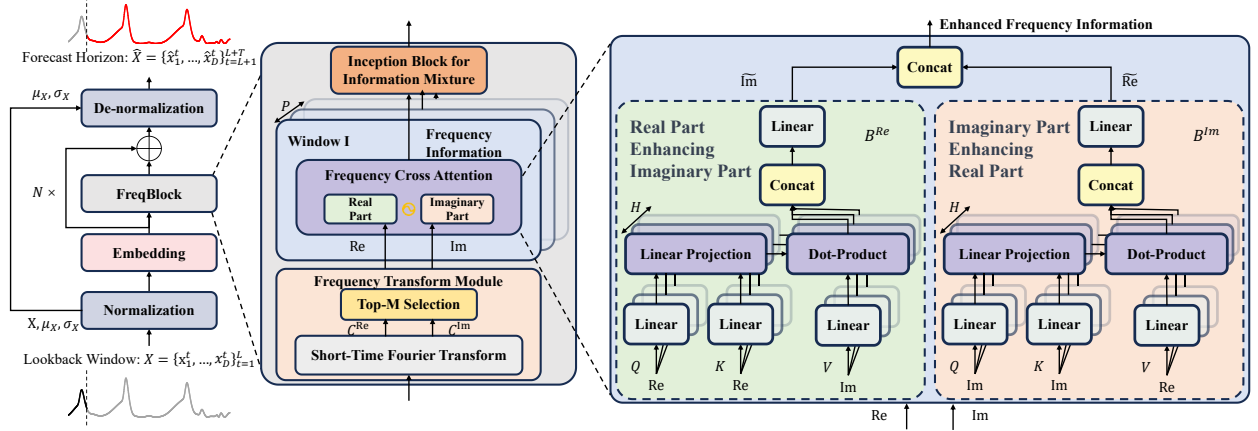


Figure 2: The structure of FreqTSE. Initially, the input lookback window,  $X \in \mathbb{R}^{D \times L}$ , undergoes normalization and embedding processes to transform it into  $X^0 \in \mathbb{R}^{E \times L}$ . This transformed input is then fed into a series of residual FreqBlocks. The output of the  $N$ -th FreqBlock, after undergoing denormalization, results in the forecasting horizon  $\hat{X} \in \mathbb{R}^{D \times T}$ . The  $n$ -th FreqBlock is defined as  $X^n = \text{FreqBlock}^n(X^{n-1}) + X^{n-1}$ . The process within each FreqBlock begins with the application of the STFT, utilizing Equation 7 to the time series data with varying window sizes. This step decomposes the data into its corresponding real and imaginary components in the frequency domain, which is then processed through the Top- $M$  frequency selection as described in Equation 9. Subsequently, the FreqBlock captures intra-variable variations using Frequency Cross Attention between the real and imaginary parts and obtain the enhanced real part  $\tilde{R}e$  and the imaginary part  $\tilde{I}m$ . Finally, the FreqBlock integrates inter-variable information through parameter-efficient Inception blocks, completing the transformation process within the block.

Inspired by the fact that the KKR's remain valid in the context of STFT, we can derive a multi-scale representation and multi-frequency components of time series through STFT. This transformation enhances computational efficiency and significantly reduces the computational cost of time series analysis [Xu et al., 2020]. Subsequently, by adaptively modeling the transformations between the real and imaginary parts, we can further capture intra-variable variations, which characterize the properties of time series variables in the frequency domain.

### 3 FreqTSE

In this section, we introduce the FreqTSE, as illustrated in Figure 2, which features a modular architecture specifically designed to model intra- and inter-variable variations in the frequency domain. The FreqTSE incorporates a series of residual-connected FreqBlocks. These FreqBlocks initially utilize the Frequency Transform Module, followed by the Frequency Cross Attention mechanism to dynamically allocate attention weights to the real and imaginary components associated with intra-variable variations. Additionally, the FreqBlocks integrate inter-variable information efficiently through parameter-efficient Inception blocks.

#### 3.1 Frequency Transform Module

The Frequency Transform Module transforms the input into frequency components using the STFT:

$$C_{j,p,k} = \text{STFT}\{X_j\}(\omega_k, \tau_p) = \sum_{t=1}^L x_j^t w_p(t - \tau_p) e^{-i\omega_k t}, \quad (7)$$

where  $X_j$  represent the time series corresponding to the  $j$ -th variable,  $w_p(\tau_p)$  denotes the  $p$ -th window function centered at  $\tau_p$  with a total of  $P$  window functions. These window functions are collectively represented as  $\{w_p\}_{p=1, \dots, P}$ . The  $k$ -th angular frequency is denoted by  $\omega_k$ .  $C_{j,p,k}$  signifies the  $k$ -th result of the STFT applied to the  $j$ -th time series using the  $p$ -th predefined window function, encapsulating the real and imaginary components. The STFT, referred to as Equation 7, can be decomposed into its real and imaginary parts utilizing  $e^{-i\omega_k t} = \cos(-\omega_k t) + i \sin(-\omega_k t) = \cos(\omega_k t) - i \sin(\omega_k t)$ . This decomposition yields the following formulations:

$$\begin{aligned}
C_{j,p,k}^{\text{Re}} &= \sum_{t=1}^L x_j^t w_p(t - \tau_p) \cos \omega_k t, \\
C_{j,p,k}^{\text{Im}} &= - \sum_{t=1}^L x_j^t w_p(t - \tau_p) \sin \omega_k t,
\end{aligned} \tag{8}$$

where  $C_{j,p,k}^{\text{Re}}$  and  $C_{j,p,k}^{\text{Im}}$  represent the  $k$ -th real and imaginary components, respectively, of the  $j$ -th time series, which are derived through decomposition using the  $p$ -th window function. Given the sparsity characteristic of the frequency domain, we opt to select only the Top- $M$  amplitude values to mitigate the computational load of the attention mechanism. Consequently, we identify the most significant real components  $C_{j,p,1}^{\text{Re}}, \dots, C_{j,p,M}^{\text{Re}}$  and imaginary components  $C_{j,p,1}^{\text{Im}}, \dots, C_{j,p,M}^{\text{Im}}$ , with  $M$  being a hyperparameter. Furthermore, by concatenating the components obtained across all  $P$  windows, we form the matrices  $\text{Re} \in \mathbb{R}^{D \times P \times M}$  and  $\text{Im} \in \mathbb{R}^{D \times P \times M}$  with  $\text{Amp}(\cdot)$  denoting the amplitude values:

$$\begin{aligned}
&\{C_{j,p,1}^{\text{Re}}, \dots, C_{j,p,M}^{\text{Re}}\}, \{C_{j,p,1}^{\text{Im}}, \dots, C_{j,p,M}^{\text{Im}}\} = \arg \text{Top-M}(\text{Amp}(C_{j,p,k}^{\text{Re}}, C_{j,p,k}^{\text{Im}})), \\
&\text{Re} = \underset{j \in \{1, \dots, D\}, p \in \{1, \dots, P\}, m \in \{1, \dots, M\}}{\text{Concatenate}} (C_{j,p,m}^{\text{Re}}), \\
&\text{Im} = \underset{j \in \{1, \dots, D\}, p \in \{1, \dots, P\}, m \in \{1, \dots, M\}}{\text{Concatenate}} (C_{j,p,m}^{\text{Im}}).
\end{aligned} \tag{9}$$

### 3.2 Frequency Cross Attention

Based on the Lemma 1, once the STFT is performed, the imaginary part can be derived from the corresponding real part, and vice versa. The crux of our method is to compute an importance score between the real and imaginary parts of each variable. To this end, we design the Frequency Cross Attention mechanism, comprising two components:  $B^{\text{Re}}$  and  $B^{\text{Im}}$ . Here,  $B^{\text{Re}}$  captures the ability of the real part to preserve the information of the imaginary part, while  $B^{\text{Im}}$  quantifies how well the imaginary part can transform into the real part, as depicted in Figure 2. To enable the model to jointly attend to information from different representation subspaces, we use  $H$  heads of cross-attention mechanisms. For the  $h$ -th head, we apply linear mappings to transform the real part  $\text{Re}$  into  $Q_h^{\text{Re}}$ ,  $K_h^{\text{Re}}$ , and  $V_h^{\text{Re}}$ , and the imaginary part  $\text{Im}$  into  $Q_h^{\text{Im}}$ ,  $K_h^{\text{Im}}$ , and  $V_h^{\text{Im}}$ :

$$\begin{aligned}
Q_h^{\text{Re}} &= \text{Re}^T W_h^{\text{Re}, Q} + b_h^{\text{Re}, Q}, Q_h^{\text{Im}} = \text{Im}^T W_h^{\text{Im}, Q} + b_h^{\text{Im}, Q}, \\
K_h^{\text{Re}} &= \text{Re}^T W_h^{\text{Re}, K} + b_h^{\text{Re}, K}, K_h^{\text{Im}} = \text{Im}^T W_h^{\text{Im}, K} + b_h^{\text{Im}, K}, \\
V_h^{\text{Re}} &= \text{Re}^T W_h^{\text{Re}, V} + b_h^{\text{Re}, V}, V_h^{\text{Im}} = \text{Im}^T W_h^{\text{Im}, V} + b_h^{\text{Im}, V}.
\end{aligned} \tag{10}$$

Here,  $W_h^{*, Q/K} \in \mathbb{R}^{D \times d_K}$ ,  $W_h^{*, V} \in \mathbb{R}^{D \times d_V}$ ,  $b_h^{*, Q/K} \in \mathbb{R}^{d_K}$ , and  $b_h^{*, V} \in \mathbb{R}^{d_V}$  are learnable parameters. Additionally,  $Q_h^*, K_h^* \in \mathbb{R}^{P \times M \times d_K}$ ,  $V_h^* \in \mathbb{R}^{P \times M \times d_V}$ . When computing  $\text{Attn}_h^{\text{Im}}$ , the representation of the real part  $\text{Re}$  is augmented with the imaginary part  $\text{Im}$ . Conversely, while calculating  $\text{Attn}_h^{\text{Re}}$ , the representation of the real part  $\text{Re}$  needs to be modulated by learnable weights in conjunction with the imaginary part  $\text{Im}$ :

$$\begin{aligned}
\text{Attn}_h^{\text{Im}}(Q_h^{\text{Im}}, K_h^{\text{Im}}, V_h^{\text{Re}}) &= \text{softmax}\left(\frac{Q_h^{\text{Im}}(K_h^{\text{Im}})^T}{\sqrt{d_K}}\right)V_h^{\text{Re}}, \\
\text{Attn}_h^{\text{Re}}(Q_h^{\text{Re}}, K_h^{\text{Re}}, V_h^{\text{Im}}) &= \text{softmax}\left(\frac{Q_h^{\text{Re}}(K_h^{\text{Re}})^T}{\sqrt{d_K}}\right)V_h^{\text{Im}}.
\end{aligned} \tag{11}$$

After computing the attention weight matrices for all  $H$  attention heads, we concatenate all  $\text{Attn}_h^{\text{Im}}$  and  $\text{Attn}_h^{\text{Re}}$  and then apply linear transformations to map them to the augmented real part  $\tilde{\text{Re}} \in \mathbb{R}^{P \times M \times d_{\text{hidden}}}$  and imaginary part  $\tilde{\text{Im}} \in \mathbb{R}^{P \times M \times d_{\text{hidden}}}$ .

$$\begin{aligned}\tilde{\text{Re}} &= \text{MultiHead}(Q^{\text{Im}}, K^{\text{Im}}, V^{\text{Re}}) = \text{Concat}(\text{Attn}_1^{\text{Im}}, \dots, \text{Attn}_H^{\text{Im}})W^{\text{Re}}, \\ \tilde{\text{Im}} &= \text{MultiHead}(Q^{\text{Re}}, K^{\text{Re}}, V^{\text{Im}}) = \text{Concat}(\text{Attn}_1^{\text{Re}}, \dots, \text{Attn}_H^{\text{Re}})W^{\text{Im}}.\end{aligned}\tag{12}$$

Here, the projections  $W^{\text{Re}}, W^{\text{Im}} \in \mathbb{R}^{Hd_V \times d_{\text{hidden}}}$  are learnable parameter matrices.

### 3.3 FreqBlock

As shown in Figure 2, we organize the FreqBlock in a residual manner to form FreqTSF, inspired by [He et al., 2016]. Specifically, for input time series  $X \in \mathbb{R}^{D \times L}$ , we first apply the normalization at the very beginning of FreqTSF to address the nonstationary characteristics resulting from varying mean and standard deviation. At the end of the FreqTSF, denormalization is applied to transform the model outputs back to the original statistics, as suggested by [Liu et al., 2022]. After normalization, the input time series becomes  $X' \in \mathbb{R}^{D \times L}$ . We then utilize a linear embedding layer to project the inputs into deep features  $X^0 \in \mathbb{R}^{E \times L}$ . For the  $n$ -th FreqBlock of the FreqTSF with the input  $X^{n-1} \in \mathbb{R}^{E \times L}$ , the process can be described as follows:

$$X^n = \text{FreqBlock}^n(X^{n-1}) + X^{n-1}.\tag{13}$$

As depicted in Figure 2, in the  $n$ -th FreqBlock, the process consists of two successive phases in the frequency domain: capturing intra-variable variations and integrating inter-variable information.

#### 3.3.1 Capturing Intra-variable Variations

In each FreqBlock, we sequentially apply the Frequency Transform Module (FTM) followed by the Frequency Cross Attention (FCA). The deep features  $X^{n-1} \in \mathbb{R}^{E \times L}$  are first processed by the FTM to obtain the Top- $M$  real and imaginary parts in the frequency domain. Subsequently, the FCA is used to connect the real part  $\tilde{\text{Re}}$  and the imaginary part  $\tilde{\text{Im}}$ , capturing intra-variable variations effectively. The formalized procedure is as follows:

$$\begin{aligned}\text{Re}^n, \text{Im}^n &= \text{FTM}^n(X^{n-1}), \\ \tilde{\text{Re}}^n, \tilde{\text{Im}}^n &= \text{FCA}^n(\text{Re}^n, \text{Im}^n),\end{aligned}\tag{14}$$

where  $\text{Re}^n, \text{Im}^n \in \mathbb{R}^{E \times P \times M}$  are the selected real and imaginary parts obtained by encoding  $X^{n-1}$  through the FTM.  $\tilde{\text{Re}}^n, \tilde{\text{Im}}^n \in \mathbb{R}^{P \times M \times d_{\text{hidden}}}$  represent the augmented real and imaginary parts.

#### 3.3.2 Integrating Inter-variable Information

After the FCA, we concatenate the real and imaginary parts and then process them through a linear mapping  $\text{Linear}^n$  with learnable parameters  $W^n \in \mathbb{R}^{d_{\text{hidden}} \times E}$  and  $b^n \in \mathbb{R}^E$ . Subsequently, we pass the result through parameter-efficient Inception blocks [Szegedy et al., 2015] denoted as  $\text{Inception}^n(\cdot)$ , which incorporates multi-scale kernels and is widely recognized as a prominent architectural component in computer vision. The learned representations serve as the output of the  $n$ -th FreqBlock, combining inter-variable information that captures correlations between variables through their mutual influences.

$$\hat{X}^n = \text{Inception}^n(\text{Linear}^n(\text{Concat}(\tilde{\text{Re}}^n, \tilde{\text{Im}}^n))),\tag{15}$$

### 3.4 Efficient computation

For each FreqBlock, the time complexity is the sum of the time complexity of the STFT in the Frequency Transform Module and the attention mechanism in the Frequency Cross Attention. The time complexity of the STFT, with a window size of  $W$ , is typically expressed as  $\mathcal{O}(W \log W)$ . This is because applying the FFT to each window requires computational effort of  $\mathcal{O}(W \log W)$ . For time series with length  $L$  and  $D$  variables, the total time complexity for  $P$  windows is  $\mathcal{O}(\sum_{p=1}^P LDW \log W)$ . Since  $W, D, P$  are usually predefined constants and are typically much smaller than  $L$ , the time complexity is finally  $\mathcal{O}(L)$ .



On the other hand, the memory complexity of FreqTSF depends on the requirements for storing intermediate results in the STFT and attention weight matrices in the Frequency Cross Attention. For the STFT, the FFT results must be stored for each window, which incurs a memory cost of  $\mathcal{O}(\sum_{p=1}^P DL)$ . Consequently, the memory complexity of the Frequency Cross Attention is mainly due to the storage of attention weights and intermediate results. However, since the Frequency Transform Module standardizes the input size for Frequency Cross Attention, represented as  $\text{Re}^n, \text{Im}^n \in \mathbb{R}^{E \times P \times M}$ , where  $E, P, M$  are predefined hyperparameters, the complexity of Frequency Cross Attention in this work is  $\mathcal{O}(EPM) = \mathcal{O}(1)$ . Given that  $D$  and  $P$  are generally predefined constants and typically much smaller than  $L$ , the memory complexity of FreqTSF is thus  $\mathcal{O}(L)$ .

## 4 Experiments

In this section, we compare the well-acknowledged and advanced models in time series forecasting, including the CNN-based model: TimesNet [Wu et al., 2023]; MLP-based models: LightTS [Zhang et al., 2022], DLinear [Zeng et al., 2023], FreTS [Yi et al., 2023] and FITS [Xu et al., 2024]; Transformer-based models: Autoformer [Wu et al., 2021], FEDformer [Zhou et al., 2022], NSformer [Liu et al., 2022], ETSformer [Woo et al., 2022], PatchTST [Nie et al., 2023], Crossformer [Zhang and Yan, 2023] and iTransformer [Liu et al., 2024]. Overall, 12 baselines are included for a comprehensive comparison.

### 4.1 Datasets

We evaluate the performance of FreqTSF on a real-world benchmark and two widely acknowledged time series simulators, covering mainstream applications in TSF: energy (the ETT dataset [Zhou et al., 2021]), medicine (the Type 1 Diabetes Mellitus Simulator (T1DMs) [Man et al., 2014]), and agriculture (the Lintul3 [Shibu et al., 2010]).

- The ETT dataset [Zhou et al., 2021] comprises data collected from electricity transformers, recorded every 15 minutes from July 2016 to July 2018. The dataset contains seven time-series variables, including load and oil temperature. Specifically, ETTh1 and ETTh2 are variant datasets with hourly granularity.
- The Type 1 Diabetes Mellitus Simulator (T1DMs) [Man et al., 2014] elucidates the temporal evolution of patient states in response to different distributions of exogenous insulin intervention doses. The U.S. Food and Drug Administration has accepted this simulator as a viable alternative to preclinical testing for evaluating novel treatment modalities for Type 1 Diabetes Mellitus. In this study, simulations are performed using default settings tailored for adult patients to generate temporal data sequences.
- Lintul3 [Shibu et al., 2010] is a classic crop growth model. In this experiment, we simulated the growth process of spring wheat in Northeast China in 2002. The dataset includes 20 time-series variables, including two dimensions of action variables and 18 dimensions of crop trait variables.

We follow standard protocol and split all datasets into training, validation, and test sets in chronological order by the ratio 6:2:2 for the ETT dataset and 7:1:2 for the other datasets. We adhere to the experimental settings established in TimesNet [Wu et al., 2023] and Autoformer [Wu et al., 2021] for a fair comparison. Expressly, for the ETTh1, ETTh2, and T1DMs datasets, the lookback window length is consistently set to 96. The forecasting lengths for both training and evaluation are fixed at 96, 192, 336, and 720. In the case of the Lintul3 dataset, the lookback window length is fixed at 30, with corresponding forecasting lengths for both training and evaluation set to 7, 14, 21, and 30.

### 4.2 Evaluation Metrics

We use the mean square error (MSE) and mean absolute error (MAE) to evaluate the accuracy of TSF, which is calculated as follows:

$$\begin{aligned} \text{MSE}(\hat{X}, X) &= \frac{1}{D \times T} \sum_{j=1}^D \sum_{t=L+1}^{L+T} (\hat{x}_j^t - x_j^t)^2 \\ \text{MAE}(\hat{X}, X) &= \frac{1}{D \times T} \sum_{j=1}^D \sum_{t=L+1}^{L+T} |\hat{x}_j^t - x_j^t| \end{aligned} \tag{16}$$

Here,  $\hat{X} \in \mathbb{R}^{D \times T}$  represents the estimated time series, while  $X$  denotes the corresponding ground-truth. The lower MSEs and MAEs indicate a better model for time series forecasting.

Table 1: The MSEs and MAEs of the time series forecasting. The cumulative number of first-place predictions for each model is summarized in the last row, serving as a comprehensive metric for evaluating overall model performance. The best results are highlighted in bold, while the second-best results are underlined.

Models		FreqTSF	iTransformer		FiTS		Crossformer		FreTS		TimesNet		PatchTST		DLinear		ETSformer		FEDformer		NSformer		LightTS		Autoformer		
	Metrics	MSE	MAE	MSE	MAE	MSE	MAE	MSE	MAE	MSE	MAE	MSE	MAE	MSE	MAE	MSE	MAE	MSE	MAE	MSE	MAE	MSE	MAE	MSE	MAE		
ETTh1	96	<b>0.214</b>	<b>0.279</b>	0.386	0.405	0.701	0.558	0.423	0.448	0.399	0.407	0.384	0.402	0.414	0.419	0.386	0.400	0.494	0.479	0.376	0.419	0.513	0.491	0.424	0.432	0.449	0.459
	192	<b>0.267</b>	<b>0.326</b>	0.441	0.436	0.718	0.570	0.471	0.474	0.450	0.438	0.436	0.429	0.460	0.445	0.437	0.432	0.538	0.504	0.420	0.448	0.534	0.504	0.475	0.462	0.500	0.482
	336	<b>0.338</b>	<b>0.369</b>	0.487	0.458	0.721	0.581	0.570	0.546	0.493	0.464	0.491	0.469	0.501	0.466	0.481	0.459	0.574	0.521	0.459	0.465	0.588	0.535	0.518	0.488	0.521	0.496
	720	<b>0.420</b>	<b>0.408</b>	0.503	0.491	0.711	0.595	0.653	0.621	0.549	0.525	0.521	0.500	0.500	0.488	0.519	0.516	0.562	0.535	0.506	0.507	0.643	0.616	0.547	0.533	0.514	0.512
	Avg	<b>0.309</b>	<b>0.350</b>	0.454	0.447	0.713	0.576	0.529	0.522	0.473	0.459	0.458	0.450	0.469	0.454	0.456	0.452	0.542	0.510	0.440	0.460	0.570	0.537	0.491	0.479	0.496	0.487
ETTh2	96	<b>0.297</b>	<b>0.346</b>	0.312	0.360	0.352	0.363	0.745	0.584	0.325	<b>0.337</b>	0.340	0.374	0.302	0.348	0.333	0.387	0.340	0.391	0.358	0.397	0.476	0.458	0.397	0.437	0.346	0.388
	192	<b>0.380</b>	<b>0.392</b>	0.410	0.410	0.428	<b>0.392</b>	0.877	<b>0.656</b>	0.463	0.395	0.402	0.414	0.388	0.400	0.477	0.476	0.430	0.439	0.429	0.439	0.512	0.493	0.520	0.504	0.456	0.452
	336	0.428	<b>0.432</b>	<b>0.455</b>	0.454	0.454	0.438	1.043	0.731	0.524	0.449	0.452	0.452	<b>0.426</b>	0.433	0.594	0.541	0.485	0.479	0.496	0.487	0.552	0.551	<b>0.626</b>	0.559	0.482	0.486
	720	<b>0.427</b>	0.479	0.487	<b>0.480</b>	0.451	0.460	1.104	0.763	0.772	0.567	0.462	0.468	0.431	<b>0.446</b>	0.831	0.657	0.500	0.497	0.463	0.474	0.562	0.560	0.863	<b>0.672</b>	0.515	0.511
	Avg	<b>0.383</b>	<b>0.407</b>	0.414	<b>0.426</b>	0.421	0.413	0.942	0.684	0.521	0.437	0.414	0.427	0.387	<b>0.407</b>	0.559	0.515	0.439	0.452	0.437	0.449	0.526	0.516	0.602	<b>0.543</b>	0.450	0.459
T1DMs	96	<b>0.06</b>	<b>0.03</b>	0.409	0.22	0.853	0.514	0.23	0.52	0.291	0.171	0.13	0.06	0.475	0.265	0.39	0.32	0.17	0.18	0.07	0.08	0.19	0.11	0.07	0.07	0.28	0.26
	192	0.08	0.11	0.429	0.273	1.044	0.618	0.19	0.59	0.257	0.199	0.12	<b>0.07</b>	0.649	0.372	0.43	<b>0.36</b>	0.34	0.33	<b>0.06</b>	0.10	0.20	0.15	0.12	<b>0.07</b>	0.56	0.45
	336	0.07	0.11	0.419	0.286	1.099	0.652	0.28	0.66	0.273	0.237	0.10	<b>0.07</b>	0.591	0.388	0.45	0.39	0.49	0.44	<b>0.06</b>	0.12	0.16	0.14	0.15	0.09	0.33	0.31
	720	<b>0.07</b>	0.11	0.382	0.265	0.962	0.518	0.22	0.71	0.233	0.206	0.11	<b>0.09</b>	0.583	0.371	0.38	0.34	0.56	0.47	0.12	0.20	0.20	0.15	0.60	0.50	0.60	0.46
	Avg	<b>0.07</b>	0.09	0.409	0.261	0.989	0.575	0.20	0.62	0.263	0.203	0.12	<b>0.07</b>	0.582	0.349	0.41	0.35	0.39	0.35	0.08	0.12	0.19	0.14	0.24	0.18	0.44	0.37
Lintul3	7	<b>2.81</b>	<b>0.42</b>	159.55	4.44	238.09	10.21	58.96	5.14	133.82	5.71	5.72	0.77	176.70	7.52	172.22	6.42	59.94	3.40	23.32	1.99	6.73	0.82	3.69	0.77	15.32	1.62
	14	<b>2.87</b>	<b>0.60</b>	259.31	12.10	411.18	15.31	60.42	5.42	250.35	11.03	12.85	0.96	325.21	11.41	366.81	9.22	43.23	2.96	10.77	1.51	19.03	1.19	13.69	1.35	75.06	3.24
	21	<b>2.49</b>	<b>0.81</b>	447.08	12.87	606.52	20.41	59.02	5.81	364.99	15.55	28.86	1.28	462.60	15.30	600.12	11.75	135.42	4.89	11.31	1.50	21.17	0.99	8.01	1.21	90.10	3.48
	30	<b>4.56</b>	<b>0.99</b>	672.39	18.37	866.90	26.64	59.87	6.03	482.04	19.97	64.22	1.85	647.39	19.44	861.78	14.02	82.08	3.58	12.48	1.52	34.37	1.18	10.40	1.34	305.86	5.92
	Avg	<b>3.18</b>	<b>0.71</b>	384.58	11.94	530.67	18.14	59.57	5.60	307.80	13.06	27.91	1.21	402.97	13.42	500.23	10.35	80.16	3.70	14.47	1.63	20.33	1.05	8.94	1.16	121.59	3.57
1 <sup>st</sup> Count			<b>30</b>		0		1		0		1		4		3		0		0		2		0		1		0

### 4.3 Implementation details

Similar to TimesNet [Wu et al., 2023], our proposed model, FreqTSF, employs L2 loss for training and is optimized using the Adam optimizer with an initial learning rate of  $10^{-3}$ . The batch size is configured to 32. All experiments are repeated five times, implemented in PyTorch, and conducted on a single NVIDIA RTX TITAN 24GB GPU.

We specify the embedding dimension  $E$  to 32, allowing us to map the input  $X \in \mathbb{R}^{D \times L}$  to  $X' \in \mathbb{R}^{32 \times L}$ . To mitigate degradation issues, we utilize  $N = 4$  FreqBlocks, incorporating residual connections. Each FreqBlock employs  $P = 3$  windows with sizes  $W = \{100, 50, 20\}$ , all configured as Hann windows. We select  $M = 10$  from the STFT results for each window to enhance computational efficiency. The dimensions  $d_K$ ,  $d_V$ , and  $d_{\text{hidden}}$  in the Frequency Cross Attention are uniformly set to 64. Within the Inception blocks, we use six kernels of varying sizes to integrate inter-variable information from distinct STFT windows. Our findings suggest that the dimensions of the hidden layers and the number of kernels do not significantly influence the performance of FreqTSF. Consequently, we undertake ablation studies on the number of FreqBlocks  $N$ , the embedding dimension  $E$ , the window  $W$ , and the selector  $M$ .

### 4.4 Main Results

The results of TSF are summarized in Table 1. We count the cumulative number of first-place predictions achieved by each model across various datasets, providing a comprehensive metric for evaluating overall model performance. The best results are highlighted in bold, while the second-best results are underlined.

Experimental results reveal that FreqTSF performs best across all benchmark datasets. Specifically, FreqTSF delivers state-of-the-art performance in 75% of all cases. On the ETTh1 dataset, FreqTSF outperforms the second-best models, FEDformer and iTransformer, by reducing the average MSE and average MAE by 30% and 22%, respectively. Although FreqTSF does not achieve the lowest MSE and MAE for all forecasting lengths on the ETTh2 dataset, it still secures the lowest average MSE and MAE. This indicates that FreqTSF’s performance is highly stable and does not fluctuate significantly with changes in forecasting lengths. On the T1DMs dataset, all methods perform relatively well. Notably, TimesNet, LightTS, and FEDformer achieve lowest MSEs and MAEs. One possible reason is that the T1DMs dataset, which reflects blood glucose levels in the human body, typically shows an upward trend before and after meals, followed by a decline to a stable level, forming a highly regular pattern. However, FreqTSF remains the best model overall, obtaining the lowest average MSE and the second-lowest average MAE. The experimental results on the Lintul3 dataset significantly demonstrate the superiority of FreqTSF. It not only achieves the highest accuracy for every forecasting length but also maintains this accuracy consistently across different lengths, thereby validating the stability of FreqTSF. We attribute this predictive accuracy and performance stability to the design of the Frequency Cross Attention, which effectively captures intra-variable variations.

### 4.5 Model Efficiency Analysis

In our model efficiency analysis, we believe that analyzing the parameter scale and GPU memory size is only necessary when a model demonstrates high accuracy. Additionally, since prediction lengths may vary across different datasets, leading to changes in parameter scale and GPU memory size, we choose to compare the parameter scale and GPU

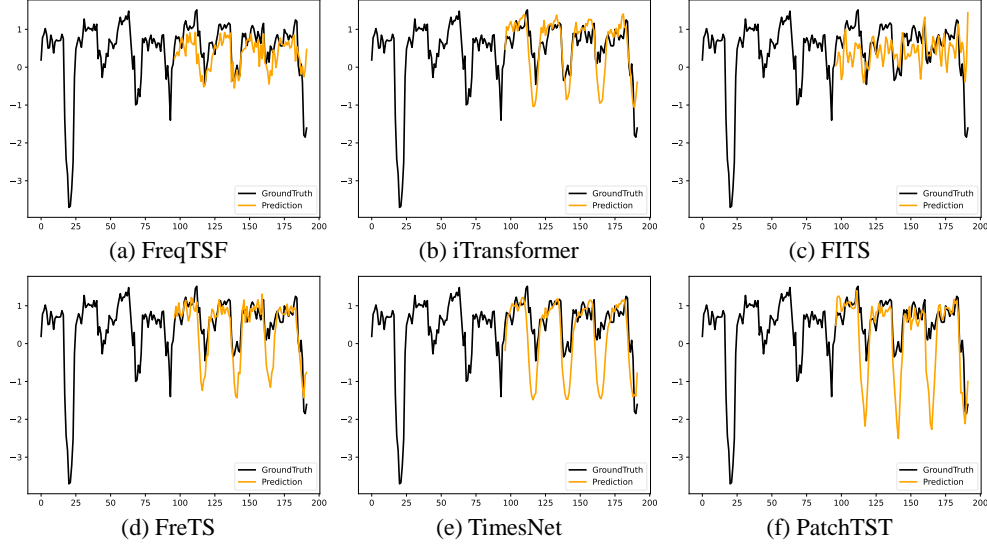


Figure 3: Visualization of ETTh1 predictions by different models under the input-96-predict-96 setting. The black lines stand for the ground truth and the orange lines stand for predicted values.

memory size of FreqTSF, PatchTST, FITS, FreTS, TimesNet, LightTS, and FEDformer on the ETTh1 dataset. These seven methods have achieved the lowest MSEs and MAEs on one of three datasets.

Among these models, our proposed FreqTSF and TimesNet exhibit nearly identical parameter sizes and GPU memory usage, with parameter sizes of 4.6MB and 4.5MB and GPU memory sizes of 1703MiB for both. On the other hand, the MLP-based models, such as LightTS and FreTS, have relatively smaller parameter sizes and GPU memory usage, averaging around 0.04MB and 1699MiB, respectively, while FITS only requires 10k parameters. However, MLP-based models may struggle to simulate time series data effectively due to their small parameter size. Conversely, PatchTST and FEDformer have parameter sizes and GPU memory usage similar to MLP-based models, but they fail to capture extreme values in time series data. We will discuss the above viewpoints visually in Section 4.6. We attribute the larger parameter size of FreqTSF primarily to the multi-window approach used in STFT, which subsequently increases the parameters required for Frequency Cross Attention. FreqTSF achieves the best performance within an acceptable single-GPU model size despite the increased parameter count.

#### 4.6 Showcases

To intuitively demonstrate the specific advantages of FreqTSF, we present a visualization of ETTh1 predictions under the input-96-predict-96 setting in Figure 3. Due to their novelty and accuracy, we selected iTransformer, FITS, FreTS, TimesNet, and PatchTST as baselines for comparison with FreqTSF. We visualized the experimental results on the ETTh1 dataset because it is a widely used public dataset, which better reflects the generalization capability of the models.

Overall, all six methods exhibit high accuracy, but there are still subtle differences. The visualization results show that FreqTSF captures details more accurately, providing precise depictions of peaks (both highest and lowest values). While iTransformer, FreTS, TimesNet, and PatchTST can perfectly fit the highest values, they struggle to accurately predict the lowest values, often predicting them to be lower than the ground-truth values. On the other hand, FITS fails to predict the highest and lowest values, with its prediction curve fluctuating around the mean of the ground-truth curve.

We believe that the reason the aforementioned five baselines fail to make accurate predictions is that they do not specifically capture intra- and inter-variable variations. FreqTSF leverages Frequency Cross Attention between the real and imaginary parts to capture intra-variable variations and uses Inception blocks to mix information and capture correlations between variables, leading to the best prediction performance.

Table 2: Ablation Studies for Modules: TSF results on ETTh1 with lookback window length  $L = 96$  and prediction length  $T = \{96, 192, 336, 720\}$ . Three variants of FreqTSF are compared with original FreqTSF.

Models	FreqTSF-FTM-FCA		FreqTSF-FCA		FreqTSF-FTM		FreqTSF	
Metrics	MSE	MAE	MSE	MAE	MSE	MAE	MSE	MAE
96	0.427	0.438	0.406	0.415	0.397	0.411	<b>0.214</b>	<b>0.297</b>
192	0.451	0.453	0.449	0.443	0.448	0.442	<b>0.267</b>	<b>0.326</b>
336	0.498	0.479	0.491	0.468	0.483	0.461	<b>0.338</b>	<b>0.369</b>
720	0.562	0.535	0.519	0.481	0.491	0.480	<b>0.420</b>	<b>0.408</b>
Avg	0.484	0.476	0.466	0.451	0.454	0.448	<b>0.309</b>	<b>0.350</b>

## 4.7 Ablation Studies

In this section, two types of ablation experiments are conducted. The module ablation studies are designed to validate the effectiveness of the Frequency Transform Module and the Frequency Cross Attention. Moreover, the ablation studies for  $M$  aim to assess the significance of information in the frequency domain.

### 4.7.1 Ablation Studies for Modules

In this section, we conduct ablation experiments on the ETTh1 dataset to validate the effectiveness of the Frequency Transform Module (FTM) and the Frequency Cross Attention (FCA). The current state-of-the-art results of FreqTSF, which utilizes both the FTM and the FCA, serve as the baseline. Three ablation variants of FreqTSF are tested: 1) FreqTSF-FTM-FCA: neither the FTM nor the FCA is used; 2) FreqTSF-FCA: the FTM and the MLP are used to capture intra-variable frequency domain information; 3) FreqTSF-FTM: the FCA is used without the FTM. The ablated FreqTSF and the SOTA model versions are compared in Table 2.

FreqTSF, including the FTM and the FCA, shows nearly 100% improvement over FreqTSF-FTM-FCA, demonstrating improvement in all four forecasting lengths. When the FTM is added, FreqTSF-FCA achieves an additional 4% improvement over FreqTSF-FTM-FCA. We posit that the FTM can effectively remove extraneous high-frequency information (such as noise) from the frequency domain, thereby facilitating the model’s understanding of trend-related information in time series data, ultimately improving accuracy. With the addition of FCA, FreqTSF-FTM achieves a 6% improvement over FreqTSF-FTM-FCA. We attribute this improvement to the ability of FCA to simulate time series modeling based on the inherent mechanism of causal systems through the establishment of real and imaginary attention. This improvement contributes to the reliability of the model. The combination of the FTM and the FCA not only achieves denoising effects but also captures the intra-variable causal characteristics of the system, resulting in state-of-the-art performance.

### 4.7.2 Ablation Studies for Top-M selection

We introduce a hyperparameter  $M$  in the Equation 9 to eliminate irrelevant information in the frequency domain. In this section,  $M = \infty$  denotes the absence of the Top- $M$  selection. The ablation analysis for  $M$  is presented in Figure 4. Experimental results on the ETTh1 dataset show that, when  $T = \{96, 192, 336, 720\}$  respectively, MSEs and MAEs tend to initially decrease (or remain constant) and then increase with increasing  $M$ . The choice of  $M$  significantly affects the final model performance, possibly because  $M$  directly influences the amount of information within deep representations. Furthermore, when  $M = \infty$ , an excessive amount of information in the frequency domain results in Frequency Cross Attention being unable to capture critical information. Conversely, when  $M = 5$ , insufficient frequency domain information hinders accurate predictions. Hence, in this study, considering both efficiency and performance, we set  $M = 10$  for TSF.

## 4.8 Hyperparameter Sensitivity

We introduce a hyperparameter  $W$  in Equation 7 to predefine the sizes of the windows in the STFT, enriching the information obtained from the Fourier transform through different windows. Furthermore, the embedding dimension  $E$  and the number of FreqBlocks  $N$  are key hyperparameters, which indicate the amount of information in deep representations and the depth of FreqTSF, respectively. Therefore, we conduct ablation experiments on the ETTh1 dataset for the number of FreqBlocks  $N$ , the embedding dimension  $E$ , and the sizes of the windows  $W$ . Table 3 provides the sensitivity analysis for the above three hyperparameters. Besides, we can also find out the following observations:

**The number of FreqBlocks  $N$ :** We observe that the impact of  $N$  on the model accuracy is not substantial. In the

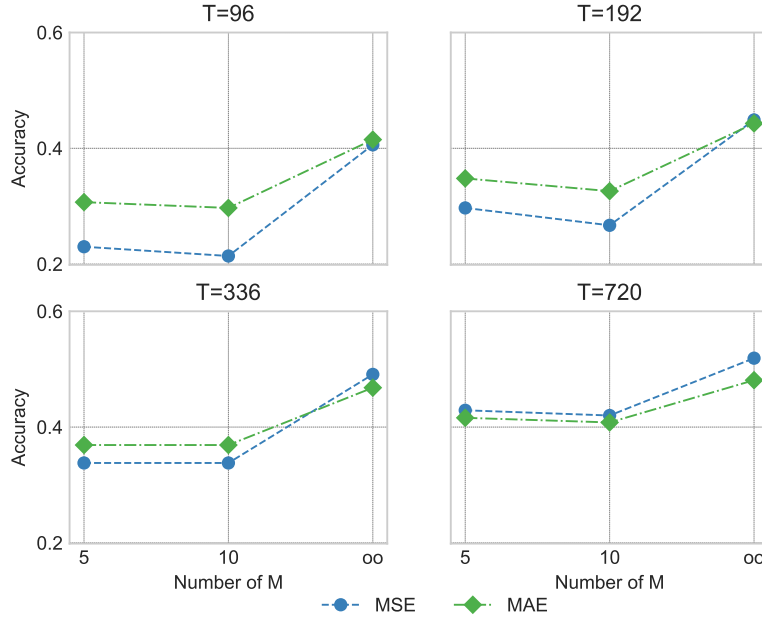


Figure 4: Ablation Studies for Top- $M$  selection. TSF results on ETTh1 dataset with input length  $L = 96$  and prediction length  $T = \{96, 192, 336, 720\}$ .

Table 3: Sensitivity analysis is performed on the hyperparameters, including FreqBlock number  $N$ , embedding dimension  $E$ , and window sizes  $W$  in FreqTSF. In particular, we perform experiments on the ETTh1 dataset to investigate the impact of these hyperparameters.

$N$	$E$	$W$	T=96		T=192		T=336		T=720	
			MSE	MAE	MSE	MAE	MSE	MAE	MSE	MAE
2	32	100,50,20	0.214	0.297	0.280	0.335	0.365	0.390	0.436	0.421
		100,50	0.230	0.303	0.294	0.347	0.344	0.373	0.437	0.422
	64	100,50,20	0.227	0.305	0.267	0.326	0.338	0.369	0.430	0.419
		100,50	0.246	0.314	0.277	0.332	0.343	0.373	0.420	0.408
4	32	100,50,20	0.229	0.305	0.285	0.338	0.341	0.371	0.433	0.419
		100,50	0.235	0.307	0.286	0.339	0.339	0.370	0.434	0.420
	64	100,50,20	0.252	0.325	0.285	0.338	0.339	0.370	0.431	0.417
		100,50	0.254	0.326	0.285	0.338	0.339	0.370	0.432	0.419

experiments with  $T = 96$  and  $T = 192$ , across the above eight experiments with fixed  $E$  and  $W$ , when  $N = 2$ , it leads to lower MSEs and MAEs in 7/8 cases. However, the experiments with  $T = 336$  and  $T = 720$  achieve lower MSEs and MAEs in 6/8 cases when  $N = 4$ . Nevertheless, the choice of  $N$  does not significantly reduce the MSEs and MAEs. Thus, we believe that the model performance is more robust to the choice of  $N$ .

**The embedding dimension  $E$ :** We find that  $E$  should also increase with the growth of the forecasting length  $T$ , and  $E$  has a notable impact on the accuracy of FreqTSF. In the experiments with  $T = 96$ , we observe that holding  $N$  and  $W$  constant, the MSEs and MAEs are lower when  $E = 32$  compared to  $E = 64$ . However, in the experiments with  $T = 192$ ,  $T = 336$ , and  $T = 720$ , FreqTSF achieves lower MSEs and MAEs when  $E = 64$ . This effect can be attributed to the fact that  $E$  directly affects the amount of information in deep representations.

**The window sizes  $W$ :** We find that the effect of the window sizes on the FreqTSF decreases as  $T$  increases. In the experiments with  $T = 96$  and  $T = 192$ , keeping  $N$  and  $E$  constant, we observe that it leads to lower MSEs and MAEs in 6/8 cases with window lengths of  $\{100, 50, 20\}$ . However, in the experiments with  $T = 336$  and  $T = 720$ , changes in the STFT window size have little effect on the MSEs and MAEs. Thus, we claim the model performance is more robust when choosing  $W$ .

## 5 Conclusion, Limitations and Future Works

In this paper, we propose FreqTSF that leverages FreqBlocks connected in a residual way, resulting in state-of-the-art performance. Each FreqBlock employs the STFT for the multi-period signal analysis, facilitating the acquisition of intra-variable variations from a frequency perspective. Inspired by KKR, we propose Frequency Cross Attention between the real and imaginary parts to obtain enhanced frequency representations and capture intra-variable variations. Inception blocks are further used to mix information to capture correlations between variables. Extensive experiments demonstrate that FreqTSF achieves superior forecasting performance with minimal resource consumption on three benchmark datasets, outperforming 12 state-of-the-art algorithms. Furthermore, FreqTSF reduces the time and memory complexity of each FreqBlock computation from  $\mathcal{O}(L^2)$  to  $\mathcal{O}(L)$ .

While FreqTSF demonstrates exceptional performance, there are still some limitations. For example, FreqTSF may incorrectly categorize mutations in time-series data as noise and overlook the accurate modeling of simple periodic curves. Therefore, to further improve and overcome the limitations, we intend to utilize both time- and frequency-domain information to improve model performance. In addition, we aim to explore large-scale pre-training methods tailored explicitly to time series applications, using FreqTSF as the underlying architecture. This approach can potentially bring significant benefits to a wide range of downstream tasks.

## 6 Acknowledgments

This study was supported in part by a grant from the National Key Research and Development Program of China [2021ZD0110900] and the National Natural Science Foundation of China [62006063].

## References

- Haixu Wu, Jiehui Xu, Jianmin Wang, and Mingsheng Long. Autoformer: Decomposition transformers with auto-correlation for long-term series forecasting. In *Advances in Neural Information Processing Systems*, 2021.
- Yong Liu, Haixu Wu, Jianmin Wang, and Mingsheng Long. Non-stationary transformers: Exploring the stationarity in time series forecasting. In *Advances in Neural Information Processing Systems*, 2022.
- Tian Zhou, Ziqing Ma, Qingsong Wen, Xue Wang, Liang Sun, and Rong Jin. FEDformer: Frequency enhanced decomposed transformer for long-term series forecasting. In *Proc. 39th International Conference on Machine Learning (ICML 2022)*, 2022.
- Gerald Woo, Chenghao Liu, Doyen Sahoo, Akshat Kumar, and Steven Hoi. Etsformer: Exponential smoothing transformers for time-series forecasting. *arXiv preprint arXiv:2202.01381*, 2022.
- Yuqi Nie, Nam H. Nguyen, Phanwadee Sinthong, and Jayant Kalagnanam. A time series is worth 64 words: Long-term forecasting with transformers. In *International Conference on Learning Representations*, 2023.
- Yong Liu, Tengge Hu, Haoran Zhang, Haixu Wu, Shiyu Wang, Lintao Ma, and Mingsheng Long. itransformer: Inverted transformers are effective for time series forecasting. In *The Twelfth International Conference on Learning Representations*, 2024.
- Zhijian Xu, Ailing Zeng, and Qiang Xu. FITS: Modeling time series with \$10k\$ parameters. In *The Twelfth International Conference on Learning Representations*, 2024.
- Francisco Martinez Alvarez, Alicia Troncoso, Jose C Riquelme, and Jesus S Aguilar Ruiz. Energy time series forecasting based on pattern sequence similarity. *IEEE Transactions on Knowledge and Data Engineering*, 23(8):1230–1243, 2010.
- Nooriya A Mohammed and Ammar Al-Bazi. An adaptive backpropagation algorithm for long-term electricity load forecasting. *Neural Computing and Applications*, 34(1):477–491, 2022.
- Li Li, Jie Sun, Liemin Ruan, and Qifa Song. Time-series analysis of continuous glucose monitoring data to predict treatment efficacy in patients with t2dm. *The Journal of Clinical Endocrinology & Metabolism*, 106(8):2187–2197, 2021.
- Heydar Khadem, Hoda Nemat, Jackie Elliott, and Mohammed Benaissa. Blood glucose level time series forecasting: Nested deep ensemble learning lag fusion. *Bioengineering*, 10(4):487, 2023.
- Umesh Saini, Rajesh Kumar, Vipin Jain, and MU Krishnajith. Univariate time series forecasting of agriculture load by using lstm and gru rnns. In *2020 IEEE Students Conference on Engineering & Systems (SCES)*, pages 1–6. IEEE, 2020.

- Yunhao Zhang and Junchi Yan. Crossformer: Transformer utilizing cross-dimension dependency for multivariate time series forecasting. In *The Eleventh International Conference on Learning Representations*, 2023.
- Kun Yi, Qi Zhang, Wei Fan, Shoujin Wang, Pengyang Wang, Hui He, Ning An, Defu Lian, Longbing Cao, and Zhendong Niu. Frequency-domain MLPs are more effective learners in time series forecasting. In *Thirty-seventh Conference on Neural Information Processing Systems*, 2023.
- George EP Box and Gwilym M Jenkins. Some recent advances in forecasting and control. *Journal of the Royal Statistical Society. Series C (Applied Statistics)*, 17(2):91–109, 1968.
- George EP Box, Gwilym M Jenkins, Gregory C Reinsel, and Greta M Ljung. *Time series analysis: forecasting and control*. John Wiley & Sons, 2015.
- Larry R Medsker and LC Jain. Recurrent neural networks. *Design and Applications*, 5(64-67):2, 2001.
- Yoshua Bengio, Patrice Simard, and Paolo Frasconi. Learning long-term dependencies with gradient descent is difficult. *IEEE transactions on neural networks*, 5(2):157–166, 1994.
- Sepp Hochreiter and Jürgen Schmidhuber. Long short-term memory. *Neural computation*, 9(8):1735–1780, 1997.
- Junyoung Chung, Caglar Gulcehre, Kyunghyun Cho, and Yoshua Bengio. Empirical evaluation of gated recurrent neural networks on sequence modeling. In *NIPS 2014 Workshop on Deep Learning, December 2014*, 2014.
- Ashish Vaswani, Noam Shazeer, Niki Parmar, Jakob Uszkoreit, Llion Jones, Aidan N Gomez, Łukasz Kaiser, and Illia Polosukhin. Attention is all you need. *Advances in neural information processing systems*, 30, 2017.
- Jacob Devlin Ming-Wei Chang Kenton and Lee Kristina Toutanova. Bert: Pre-training of deep bidirectional transformers for language understanding. In *Proceedings of naacL-HLT*, volume 1, page 2, 2019.
- Alexey Dosovitskiy, Lucas Beyer, Alexander Kolesnikov, Dirk Weissenborn, Xiaohua Zhai, Thomas Unterthiner, Mostafa Dehghani, Matthias Minderer, Georg Heigold, Sylvain Gelly, et al. An image is worth 16x16 words: Transformers for image recognition at scale. In *International Conference on Learning Representations*, 2020.
- Haixu Wu, Tengge Hu, Yong Liu, Hang Zhou, Jianmin Wang, and Mingsheng Long. Timesnet: Temporal 2d-variation modeling for general time series analysis. In *International Conference on Learning Representations*, 2023.
- Christian Szegedy, Wei Liu, Yangqing Jia, Pierre Sermanet, Scott Reed, Dragomir Anguelov, Dumitru Erhan, Vincent Vanhoucke, and Andrew Rabinovich. Going deeper with convolutions. In *Proceedings of the IEEE conference on computer vision and pattern recognition*, pages 1–9, 2015.
- Tianping Zhang, Yizhuo Zhang, Wei Cao, Jiang Bian, Xiaohan Yi, Shun Zheng, and Jian Li. Less is more: Fast multivariate time series forecasting with light sampling-oriented mlp structures. *arXiv preprint arXiv:2207.01186*, 2022.
- Ailing Zeng, Muxi Chen, Lei Zhang, and Qiang Xu. Are transformers effective for time series forecasting? 2023.
- Henri J Nussbaumer and Henri J Nussbaumer. *The fast Fourier transform*. Springer, 1982.
- William T Cochran, James W Cooley, David L Favin, Howard D Helms, Reginald A Kaenel, William W Lang, George C Maling, David E Nelson, Charles M Rader, and Peter D Welch. What is the fast fourier transform? *Proceedings of the IEEE*, 55(10):1664–1674, 1967.
- William L Briggs and Van Emden Henson. *The DFT: an owner’s manual for the discrete Fourier transform*. SIAM, 1995.
- Zoran Cvetkovic. On discrete short-time fourier analysis. *IEEE transactions on signal processing*, 48(9):2628–2640, 2000.
- Lutfiye Durak and Orhan Arikan. Short-time fourier transform: two fundamental properties and an optimal implementation. *IEEE Transactions on Signal Processing*, 51(5):1231–1242, 2003.
- Kamran Karimi and Howard J Hamilton. Distinguishing causal and acausal temporal relations. In *Pacific-Asia Conference on Knowledge Discovery and Data Mining*, pages 234–240. Springer, 2003.
- Frederick W King. *Hilbert Transforms: Volume 2*, volume 2. Cambridge University Press, 2009.
- Vaclav Cizek. Discrete hilbert transform. *IEEE Transactions on Audio and Electroacoustics*, 18(4):340–343, 1970.
- D Benitez, PA Gaydecki, A Zaidi, and AP Fitzpatrick. The use of the hilbert transform in ecg signal analysis. *Computers in biology and medicine*, 31(5):399–406, 2001.
- Eric W Weisstein. Convolution theorem. *From MathWorld-A Wolfram Web Resource*, 2006a. URL <http://mathworld.wolfram.com/ConvolutionTheorem.html>, 2014.
- Kai Xu, Minghai Qin, Fei Sun, Yuhao Wang, Yen-Kuang Chen, and Fengbo Ren. Learning in the frequency domain. In *Proceedings of the IEEE/CVF conference on computer vision and pattern recognition*, pages 1740–1749, 2020.

- Kaiming He, Xiangyu Zhang, Shaoqing Ren, and Jian Sun. Deep residual learning for image recognition. In *Proceedings of the IEEE conference on computer vision and pattern recognition*, pages 770–778, 2016.
- Haoyi Zhou, Shanghang Zhang, Jieqi Peng, Shuai Zhang, Jianxin Li, Hui Xiong, and Wancai Zhang. Informer: Beyond efficient transformer for long sequence time-series forecasting. In *Proceedings of the AAAI conference on artificial intelligence*, volume 35, pages 11106–11115, 2021.
- Chiara Dalla Man, Francesco Micheletto, Dayu Lv, Marc Breton, Boris Kovatchev, and Claudio Cobelli. The uva/padova type 1 diabetes simulator: new features. *Journal of diabetes science and technology*, 8(1):26–34, 2014.
- Muhammed E Shibu, Peter A Leffelaar, Herman Van Keulen, and Pramod K Aggarwal. Lintul3, a simulation model for nitrogen-limited situations: Application to rice. *European Journal of Agronomy*, 32(4):255–271, 2010.